AGU PUBLICATIONS

Geophysical Research Letters

RESEARCH LETTER
10.1002/2017GL072649

Key Points:
- Implement a novel and more objective metric for midlatitude waves and extremes
- Attribution study suggests no midlatitude-wide increase of wave activity under the abrupt decline of Arctic sea ice
- Show evidence that sea ice loss over Barents-Kara Sea and SST trend both contribute to the increase of local wave activity near Siberia

Supporting Information:
- Supporting Information S1

Correspondence to:
J. Lu,
Jian.Lu@pnnl.gov

Citation:
Xue, D., J. Lu, L. Sun, G. Chen, and Y. Zhang (2017), Local increase of anticyclonic wave activity over northern Eurasia under amplified Arctic warming, *Geophys. Res. Lett.*, *44*, doi:10.1002/2017GL072649.

Received 14 JAN 2017
Accepted 22 MAR 2017
Accepted article online 27 MAR 2017

Local increase of anticyclonic wave activity over northern Eurasia under amplified Arctic warming

Daokai Xue[1], Jian Lu[2], Lantao Sun[3,4], Gang Chen[5], and Yaocun Zhang[1]

[1]School of Atmospheric Sciences, Nanjing University, Nanjing, China, [2]Atmospheric Sciences and Global Change Division, Pacific Northwest National Laboratory, Richland, Washington, USA, [3]CIRES, University of Colorado Boulder, Boulder, Colorado, USA, [4]PSD, ESRL, NOAA, Boulder, Colorado, USA, [5]Department of Earth and Atmospheric Sciences, UCLA, Los Angeles, California, USA

Abstract In an attempt to resolve the controversy as to whether Arctic sea ice loss leads to more midlatitude extremes, a metric of finite-amplitude wave activity is adopted to quantify the midlatitude wave activity and its change during the period of the drastic Arctic sea ice decline in both ERA Interim reanalysis data and a set of Atmospheric Model Intercomparison Project-type of model experiments. Neither the ensemble mean response to the trend in the SST nor that to the declining trend of Arctic sea ice can replicate the sizable midlatitude-wide increase in the total wave activity (A_e) observed in the reanalysis, leaving its explanation to the atmospheric internal variability. On the other hand, both the diagnostics of the flux of the local anticyclonic wave activity (LAWA) and atmospheric general circulation model experiments lend evidence to a possible linkage between the sea ice loss near the Barents and Kara Seas and the increasing trend of LAWA over the northern part of the central Eurasia and the associated impacts on the frequency of temperature extremes.

1. Introduction

Recent decades have seen accentuated warming and precipitous decline of sea ice in the Arctic, in keeping with the so-called Arctic amplification anticipated from the increasing greenhouse gas forcing [*Holland and Bitz*, 2003; *Screen and Simmonds*, 2010; *Graversen et al*., 2008; *Serreze et al*., 2009]. Accompanying the Arctic change are the more frequently observed winter weather extremes like cold snaps and snow storms in the Northern Hemisphere midlatitudes since the early 1990s, especially over the eastern United States and central Asia [*Min et al*., 2011; *Coumou and Rahmstorf*, 2012; *Coumou et al*., 2013; *Westra et al*., 2013]. Some studies [*Francis and Vavrus*, 2012; *Cohen et al*., 2013, 2014] attempted to assign causation from the Arctic sea ice melting to the midlatitude extremes, and thus a controversy ensues regarding whether the Arctic amplification has led to the more frequent midlatitude extremes [*Barnes and Screen*, 2015; *Overland et al*., 2011; *Liu et al*., 2012; *Gerber et al*., 2014; *Li et al*., 2015; *Sun et al*., 2016; *McCusker et al*., 2016]. The proponents of the Arctic-midlatitude connection [*Francis and Vavrus*, 2012, 2015; *Cohen et al*., 2014] suggested that Rossby waves propagating in a weakened westerly jet tends to slowdown and become meridionally amplified, thus favoring more extreme weather conditions in the context of Arctic amplification. Other studies [*Barnes*, 2013; *Screen and Simmonds*, 2013] questioned their methodology and pointed out that the claimed increase in waviness might be an artifact due to the metric used for quantifying the wave amplitude and the interpretation thereof. Furthermore, the proposition for wave amplitude amplification was challenged by the notion that the relationship above between the wave activity and zonal jet holds only for internal variability but may break down under externally imposed thermal forcing such as Arctic amplification [*Hassanzadeh and Kuang*, 2015; *Chen et al*., 2015].

Less controversial is the possible influence of the Arctic sea ice loss on weather and temperatures over the adjacent continents [e.g., *Tang et al*., 2013; *Overland et al*., 2015; *Screen et al*., 2013; *Kretschmer et al*., 2016]. Reduction in autumn-winter Arctic sea ice, especially in the Barents-Kara Sea, has been linked to more frequent and persistent anticyclonic circulation over northern Eurasia, inducing cold events to its southeastern flank [*Mori et al*., 2014; *Petoukhov and Semenov*, 2010; *Inoue et al*., 2011; *Horton et al*., 2015; *Kug et al*., 2015]. This is consistent with the finding that the amplification of quasi-stationary waves tends to preferentially occur in eastern Europe and central Asia [*Screen and Simmonds*, 2014].

However, studies summarized above used disparate metrics for the midlatitude waviness and/or extremes; most of them are empirical and lacking an interpretation from the perspective of atmospheric dynamics;

some explanation may lead to unnecessary confusion. In this study, we utilize an objective metric founded on geophysical fluid dynamical principles to quantify the changes in the midlatitude waviness and their possible attribution to Arctic sea ice melting through a suite of atmospheric general circulation model (AGCM) simulations. The said metric is the local variant of the finite-amplitude wave activity, which can be readily partitioned into the mean gradient and eddy meridional scale, thus resolving the caveat of the metrics that tend to confuse the role of background temperature warming with that of the eddy meridional scale in the wave activity.

2. Methodology and Model Experiments

2.1. Local Wave Activity

Finite-amplitude wave activity is developed as an objective measure for the areal displacement of a physical quantity that shows broad monotonicity in its spatial distribution. Local wave activity (LWA) is a natural extension of the finite-amplitude wave activity toward locality. The exact definition of wave activity for potential vorticity and the related dynamical properties has been detailed in *Nakamura and Solomon* [2010] and *Nakamura and Zhu* [2010]. Recently, *Huang and Nakamura* [2015] developed a local variant of wave activity—LWA—and the related budget for local wave phenomena like wave breakings and blockings; *Chen et al.* [2015] further extended the concept of LWA to less conserved quantity (500 hPa geopotential height, denoted by z_{500}) to facilitate its broader application. The latter approach for z_{500} is adopted for this study.

Specifically, for z_{500} that has broad monotonic distribution with latitude, one can select a contour value Z_{500} (upper case for its Lagrangian nature following the contour) and define an equivalent latitude ϕ_e in the Northern Hemisphere such that the area S bounded by the value Z_{500} toward the North Pole is

$$S(Z_{500}) = \iint_{z \geq Z_{500}} a^2 \cos\phi \, d\lambda \, d\phi \,, \tag{1}$$

where λ is longitude, ϕ is latitude, and a is the radius of Earth. A one-to-one relationship between ϕ_e and Z_{500} values can then be established:

$$\phi_e(Z_{500}) = \arcsin\left[1 - \frac{S(Z_{500})}{2\pi a^2}\right]. \tag{2}$$

Introducing an eddy component $\hat{z} = z_{500} - Z_{500}$, the southward and northward LWA at longitude λ and equivalent latitude ϕ_e can be defined as

$$A_S(\lambda, \phi_e) = \frac{a}{\cos\phi_e} \int_{\hat{z} \leq 0, \phi \leq \phi_e} \hat{z}(\lambda, \phi) \cos\phi d\lambda d\phi \,, \tag{3}$$

$$A_N(\lambda, \phi_e) = \frac{a}{\cos\phi_e} \int_{\hat{z} \geq 0, \phi \geq \phi_e} \hat{z}(\lambda, \phi) \cos\phi d\lambda d\phi \,, \tag{4}$$

respectively. Defined as such, both $-A_S$ and A_N are positive definite, with the former describing the cyclonic wave activity residing to the south of the equivalent latitude ϕ_e and the latter the anticyclonic wave activity (LAWA) to the north of ϕ_e. Large and persistent A_N is often related to atmospheric blocking, and the spatial correspondence between their climatological distributions has been noted (Patrick Martineau, personal communication). The sum of $-A_S$ and A_N recovers the total wave activity $A_e(\phi_e) = -A_S + A_N$, which is a function of ϕ_e only, resuming the original meaning of wave activity measuring the total waviness in contour Z_{500}. A simple dimensional analysis suggests that the total wave activity can be scaled as $A_e \sim \frac{1}{2} l^2 \cdot \frac{dZ_{500}}{dy}$. As such the wave activity can be thought of as the result of the stirring of tracer z_{500} with a background gradient dZ_{500}/dy by a meridional disturbance of scale l, thus naturally partitioned into a thermodynamic factor (former) and a dynamical one (latter). For a typical meridional height gradient $\frac{\partial Z_{500}}{\partial \phi_e} \sim 8$ m/° latitude, a meridional stirring by $\delta\phi \sim 15°$ latitude implies a wave activity of $A \sim 10^8$ m^2.

We have also developed a budget for LAWA, which comprises a term for the convergence of LAWA flux and a diabatic sink/source. The details of the derivation of the budget and the results of the budget analysis are reported in the supporting information.

2.2. AGCM Experiments and Reanalysis Data Set

In this investigation, we make use of the daily output from two groups of existing AGCM experiments described in *Perlwitz et al.* [2015] and *Deser et al.* [2015], respectively. The former comprises two sets of

Table 1. Overview of Model Experiments

Experiments	SST	SIC	Radiative Forcing	Model (No. of Members/Years)
AMIP Historical	1990–2014	1990–2014	1990–2014	ECHAM5 (30)
AMIP SST	1990–2014	1979–1989 climatology	1990–2014	ECHAM5 (30)
ICE_CAM_20	1980–1999	1980–1999 (historical)	2000	CAM4 (260 years)
ICE_CAM_21	1980–1999	2080–2099[a] (RCP8.5)	2000	CAM4 (260 years)

[a]SST condition accompanying the 2080–2099 Arctic sea ice loss is specified at the grid cells where the ice concentration is lower than that in the late 20th century.

30-member Atmospheric Model Intercomparison Project (AMIP)-style simulations by using European Centre/Hamburg version 5 (ECHAM5): one denoted *AMIP Historical* forced by the observed/projected radiative forcing, observed monthly sea surface temperature (SST), and sea ice concentrations (SIC) [*Hurrell et al*., 2008] and the other *AMIP SST* forced by SST and radiative forcings identical to AMIP Historical but a repeating climatological seasonal cycle of sea ice for 1979–1989 (see *Perlwitz et al*. [2015] for more details). The difference between the 30-member ensembles of AMIP Historical and AMIP SST, denoted as AMIP ΔSIC, can then be attributed to the variability of Arctic sea ice. The 1990–2014 linear trends of net upward surface turbulence heat flux (i.e., the sum of latent heat flux and sensible heat flux) averaged over the Arctic Ocean are compared among a reanalysis, AMIP Historical and AMIP ΔSIC experiments in Figure S1 in the supporting information. There is a reasonable agreement among them in the seasonality of the trend of net surface heat flux, as well as the magnitude of the wintertime flux, which peaks at ~40 W m^{-2} in December in all the three cases. This reasonable agreement lends us some confidence in the representativeness of the forcing to the atmosphere from the Arctic sea ice melting.

For the impact of future Arctic sea ice melting, we analyze a pair of time-slice experiments with Community Atmosphere Model version 4 (CAM4), each 260 years long, forced by a repeating seasonal cycle of sea ice representing the 20th century sea ice condition (averaged between 1980 and 1999 from Community Climate System Model version 4 (CCSM4) historical runs) and the 21st century condition (averaged between 2080 and 2099 from CCSM4 Representative Concentration Pathway 8.5 (RCP8.5) runs), respectively. Over regions of reduced sea ice concentration, the RCP8.5 SST averaged over the period of 2080–2099 is used. Therefore, the difference (SIM hereafter) between the two cases (denoted as ICE_CAM_20 and ICE_CAM_21, respectively) isolates the atmospheric response not only to the reduction of Arctic sea ice but also to the SST warming over the open water as the by-product of sea ice melting. Table 1 summarizes these two groups of experiments.

Daily mean surface air temperature and 500 hPa geopotential height at spatial resolution of 1.125° longitude × 1.125° latitude from the European Centre for Medium-Range Weather Forecasts Interim (ERA-I) project [*Dee et al*., 2011] are used in the present study as a reference for the observation.

3. Results

3.1. Trend of Local Wave Activities in Reanalysis and Model Simulations

To evaluate whether Arctic sea ice loss can induce a broad change in the midlatitude waviness, we start with examining the trend of the seasonal mean total wave activity A_e in the ERAI reanalysis and AMIP-type experiments by using ECHAM5. The trend is computed by using least squares linear fitting. A significant upward trend (based on two-tailed Student's *t* test) of wintertime (December–February, DJF hereafter) A_e during 1990/1991–2013/2014 is detected in ERA-Interim (Figure 1a, black line), especially for the latitude poleward of 50°N, indicating enhanced midlatitude wave activities. This midlatitude increase occurs despite the decrease in the reduction of the Lagrangian gradient dZ_{500}/dy (consistent with the overall weakening of the poleward gradient of the lower tropospheric temperature), implicative of an even greater increase in the stirring length squared l^2 (computed as $l^2 \sim 2\, A_e / \frac{dZ_{500}}{dy}$; Figure 1c). However, none of the features in ERAI can be replicated by the ensemble mean trend in the AMIP experiments; experiment AMIP ΔSIC even produces a weak negative A_e trend in high latitudes. The weak trends in the model should not be attributed to the model deficiencies in simulating the wave activity, as Figure S2 shows the climatological mean distribution of the winter A_e and the related factors for both ERA-I the AMIP Historical experiment and the

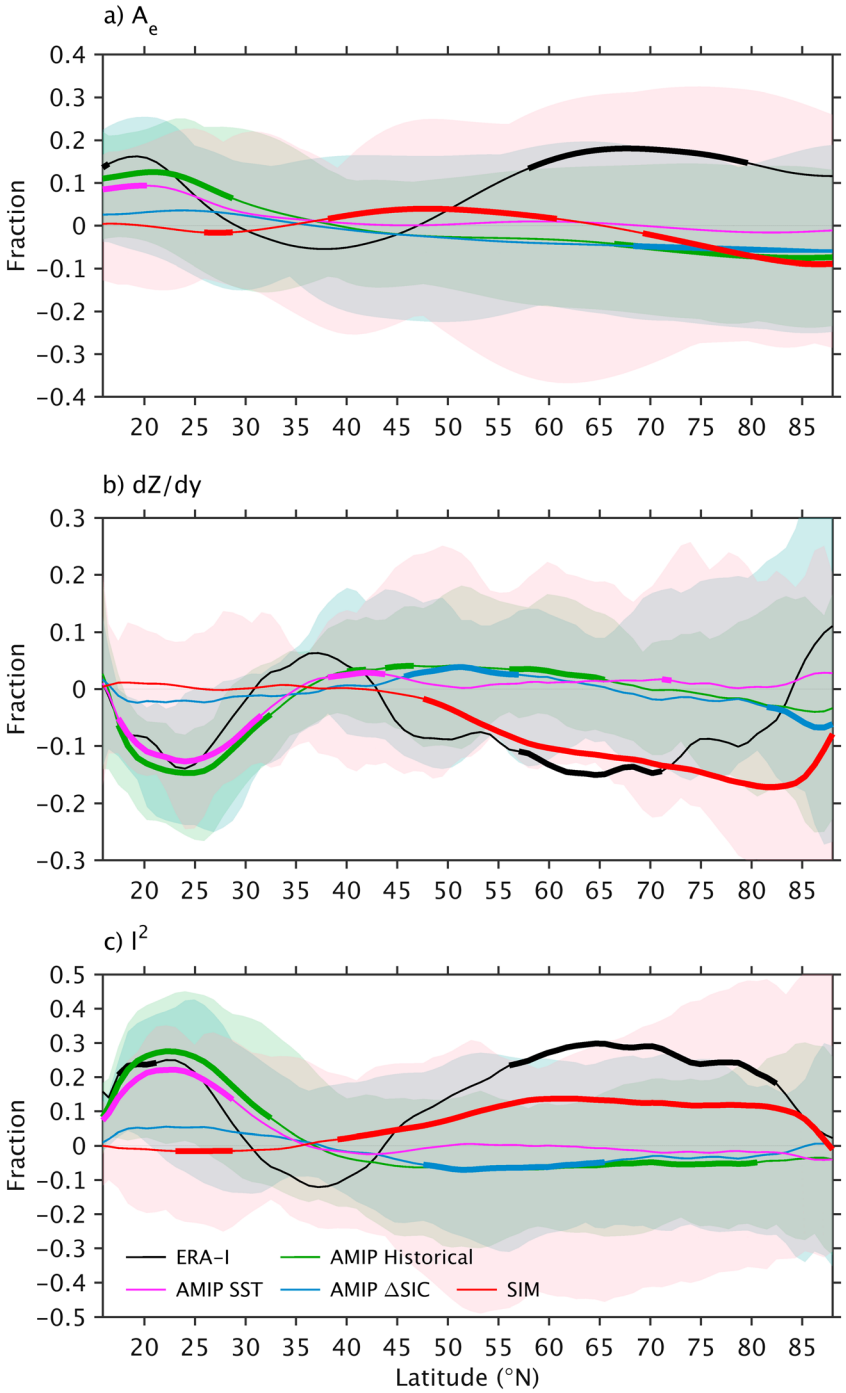

Figure 1. Fractional linear trend during the period of 1990–2013 in (a) A_e, (b) Lagrangian gradient dZ_{500}/dy, and (c) stirring length l^2 from ERA-I reanalysis (black), AMIP Historical (green), AMIP SST (magenta), and AMIP ΔSIC (blue) experiments. The red line in each panel is the fractional change of A_e, dZ_{500}/dy, and l^2 between experiments ICE_CAM_20C and ICE_CAM_21C (i.e., SIM). All are computed based on the DJF winter mean values. The latitudinal range where the trend is statistically significant at 95% confidence level based on Student's *t* test is highlighted in bold. The transparent shading indicates the range of the spread of the ensemble members in AMIP Historical (green), AMIP SST (magenta), and AMIP ΔSIC (blue) experiments.

agreement between the model and reanalysis is reassuring. All the trends in the three quantities from ERAI fall within the plumes of the ensemble spread of AMIP Historical experiment, whereas two-tailed Student's *t* tests based on the DJF mean data indicate the trends, are significant (at 95% level) with respect to the background interannual noise between 55° and 75°N. Note that the null hypothesis for the Student's *t* test

is evaluated against the noise level in the DJF seasonal mean time series, not the internal daily noise. Inspecting all the ensemble members of the AMIP experiments, we found one member that can produce trends resembling those from the ERAI in both magnitude and meridional structure (Figure S3), suggesting that ECHAM5 can accommodate a realization of wave activity as the observed one.

On the other hand, the AMIP model experiments can capture well the observed trends in the subtropics: the increases in I^2 and A_e and the decrease in dZ_{500}/dy appear attributable to the SST forcing in the AMIP experiments (Figure 1, green and magenta lines). It is also of interest to note that the difference between ICE_CAM_21 and ICE_CAM_20 using CAM4 (red lines in Figure 1), representing the impact of the future Arctic sea ice loss, shows increases in I^2 and decrease in dZ_{500}/dy resembling the ERA-I trends in middle-to-high latitudes. However, the related total wave activity difference, after the cancellation between the two factors, is well within the range of the intermember spread and shows little resemblance to the trend in ERA-I. In view of the situation that neither ECHAM5 forced by the historical sea ice forcing nor the CAM4 forced by the future projected sea ice condition can capture the magnitude of the extratropical increase in A_e, we cannot reject the null hypothesis that the extratropical trend in A_e seen in ERA-I is the result of internal variability.

When it comes to the trend of LAWA, the observed two centers of significant increase of A_N (representing anticyclonic wave anomalies) over north central Eurasia and northeastern Pacific can be captured by the AMIP Historical experiment, but with reduced magnitude (compare Figures 2a and 2b). Decomposing the modeled signal into that due to SST and sea ice, we find that the increase over northeastern Pacific can be largely attributed to the SST forcing, while both SST and sea ice play a part in the A_N trend over central northern Eurasia (Figures 2c and 2d). As a major La Niña event can recurrently lead to a high A_N anomaly over northeastern Pacific (see Figure S3 and correlations therein), the A_N trend there is likely the result of the La Niña-like SST trend in the central and eastern equatorial Pacific since the early 1990s [e.g., *Delworth et al*., 2015]. Under the Arctic sea ice condition of the late 21st century (representing a much greater sea ice forcing compared to historical reduction), the A_N increase over Eurasia simulated by CAM4 can reach similar magnitude to the observation (Figure 2e), giving rise to detectable signal on the temperature extremes over the impact areas (to be elaborated in the next section).

Focusing on the feature of the A_N increase over Eurasian region, we further define a LAWA index (I_{A_N}) by spatially averaging A_N over (50°–70°E, 50°–70°N), and the resultant time series for ERA-I reanalysis and AMIP simulations are presented in Figure 3. Consistent with the A_N trend pattern shown in Figure 2, both ERA-I reanalysis and the two AMIP experiments exhibit an upward trend in I_{A_N}. Compared to the large internal variability of I_{A_N} in ERA-I reanalysis, the interannual fluctuations of the model ensemble mean I_{A_N} is much muted, rendering a marginal significance (at 95% level) to the trend in the ensemble mean I_{A_N} in AMIP Historical. Note, however, that the standard deviation of I_{A_N} averaged over the individual members of AMIP Historical ensemble (0.29×10^8 m^2) is much larger than that in ERA-I (0.17×10^8 m^2). This trend seems to arise from both the SST (Figure 3, magenta line) and Arctic sea ice forcing (blue line) during 1990–2013. Interestingly, a large positive I_{A_N} anomaly is often associated with a La Niña SST condition in the central eastern Pacific and vice versa in both ERA-I and AMIP SST experiments. This points to a possibility that El Niño–Southern Oscillation (ENSO) teleconnection can impact on the transient weather activity as remote as central Eurasia, an aspect of ENSO worth further investigation.

The evidence from the AMIP experiments for the teleconnection between the Arctic sea ice melting and the Eurasian A_N trend is only suggestive at most. In the supporting information, we compute the divergent flux of LAWA $\boldsymbol{F}_{A_N} = (\boldsymbol{F}_u, \boldsymbol{F}_v)$ and its corresponding convergence for both ERA-I data and the difference between experiments ICE_CAM_20C and ICE_CAM_21C. The pattern of the ERA-I trend during the period of 1990–2013 (Figure S5a) indeed suggests a wave propagation pathway from the Arctic to the central Eurasia, while this pathway is less evident in the change forced by the future sea ice melting (i.e., in SIM).

3.2. Temperature Impact of A_N Over Eurasia

Given the fact that a large positive A_N is often associated with anticyclonic blocking [*Chen et al*., 2015] that advects cold Arctic air southward and warm air poleward [e.g., *Sillmann et al*., 2011], it is conceivable that the increasing trend of A_N over northern central Eurasia may bring about detectable changes in the distribution of temperature extremes nearby. Making use of the ERA-I reanalysis, we first composite the surface temperature anomalies that are congruent with the large I_{A_N} and identify two locales that are subject to its

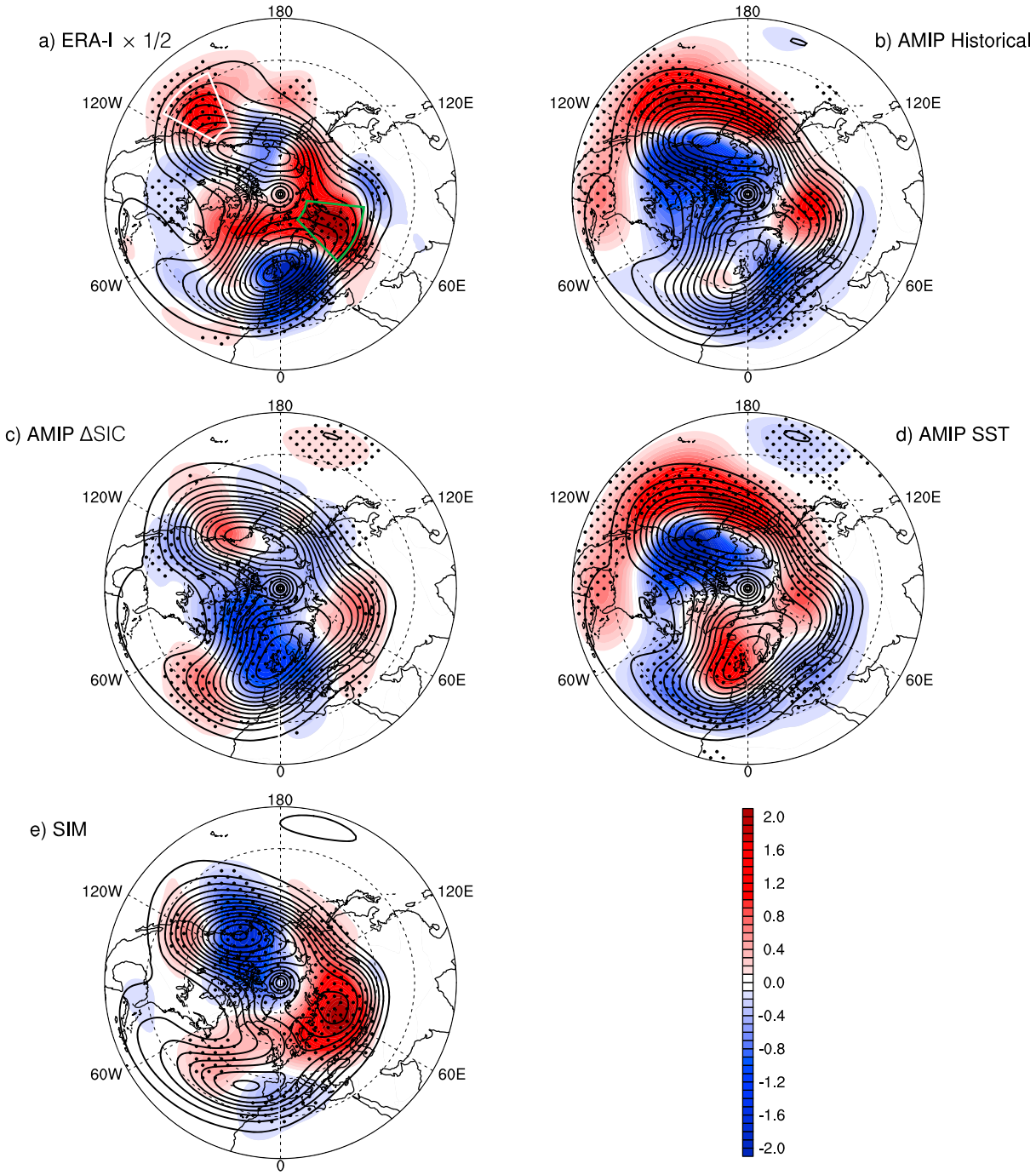

Figure 2. Distributions of the background DJF winter mean A_N (contours, C.I.: 10^8 m^2) and its linear trend (shaded; unit in 10^7 m^2) over the period of 1990–2013 in (a) ERA-I (with the trend halved for comparison purpose), (b) AMIP Historical experiment, (c) AMIP ΔSIC experiment, and (d) AMIP SST experiment. (e) The model climatological DJF mean A_N and its difference between experiments ICE_CAM_21 and ICE_CAM_20. The black dots in each panel stand for the significant trend or difference at 95% confidence level using Student's *t* test. The green and white boxes in Figure 2a demarcate the regions where the A_N time series in Figures 3 and S3 are taken, respectively.

advective effect: an area near the Barents-Kara Sea (50°–70°E, 70°–80°N) and one near central Asia (75°–95°E, 48°–58°N). These are the two regions where the large I_{A_N} trend may be manifested in the respective temperature distribution. Then we examine the change in the probability distribution of the daily surface temperature over these two areas by computing the linear trend (in ERA-I) or difference (between model experiments) of frequency of occurrence at each temperature bin.

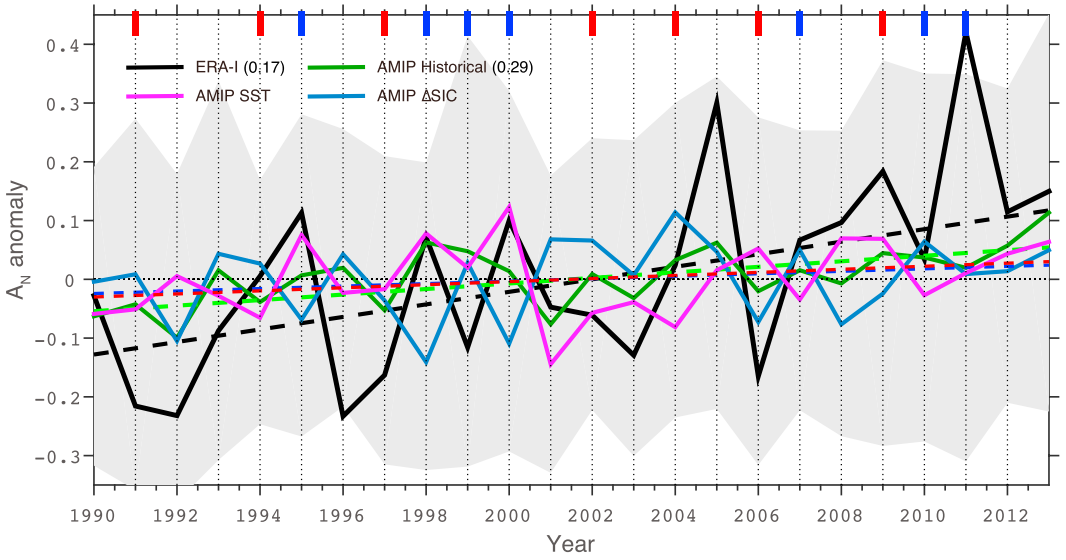

Figure 3. Time series of DJF mean A_N anomaly (unit in 10^8 m^2) over Eurasian region (green box marked in Figure 2a) in ERA-I (black), AMIP Historical experiments (green), AMIP ΔSIC experiment (blue), and AMIP SST experiment. The dashed lines that stand for the trend of A_N for 1990–2013. El Niño (La Niña) years (according to the Niño-3.4 index provided by the Climate Prediction Center) are marked by red (blue) bars on the top of the box. The gray shading indicates 1 standard deviation of the A_N index simulated by the 30 ensemble members of AMIP Historical experiments. The numbers in the parenthesis are the standard deviations over the period examined.

As anticipated from the large increase of I_{A_N}, a probability dipole with less frequent cold events and more frequent warm events is found in the 1990–2014 trend of the probability distribution function (PDF) of the ERA-I surface temperature over the Barents-Kara Sea region (Figure 4a), while an opposite probability dipole is found over the central Asia region (Figure 4b). Both dipolar PDF trends are statistically significant with respect to the PDFs constructed by randomly sampling the DJF daily temperature over the two regions 10,000 times. The same analysis of the temperature PDF for experiment AMIP ΔSIC shows similar dipoles in character, but only the PDF dipole for the northern region is statistically significant (Figure 4c). Much of the PDF dipole for the northern region should not be attributed to the increase of I_{A_N}, since the SST there experienced a large warming [*Sun et al.*, 2016] and the warming has already been prescribed in the model experiments by design. However, under Arctic sea ice loss by the late 21st century, the CAM4 time slice experiments do capture qualitatively similar PDF dipoles for both southern and northern regions as observed (Figures 4e and 4f). The counterintuitive corollary is that the sea ice loss and the related warming trend over Barents-Kara Sea, if continuing following the RCP8.5 scenario and acting in isolation, can potentially bring more cold extremes to central Asia.

4. Conclusion

A novel metric for measuring the midlatitude wave activity is devised and used to evaluate the possible role of the precipitous Arctic sea ice melt during recent decades in the increasing frequency of midlatitude weather extremes. The said metric is the finite-amplitude wave activity A_e developed recently from the geophysical fluid dynamics community and applied to 500 hPa geopotential height; it can be readily decomposed into the changes in the mean gradient and eddy stirring scale. The local extension of it can be used to quantify the wave magnitude locally. Evaluating the trends of the both total and local wave activities from ERA-I reanalysis against those from AMIP-type AGCM experiments shows that the observed Arctic sea ice loss leads to no midlatitude-wide increase in the total wave activity, while locally, the reduction of the sea ice over Barents-Kara Sea can induce an increase in LAWA over central northern Eurasia. This southward teleconnection finds some supports from diagnosing the flux of the LAWA. In another set of time slice experiments forced by the sea ice decline representing the condition of late 21st century, the LAWA response over Eurasia is amplified and can lead to significant modulation on the distribution of the temperature extremes over the impacted areas.

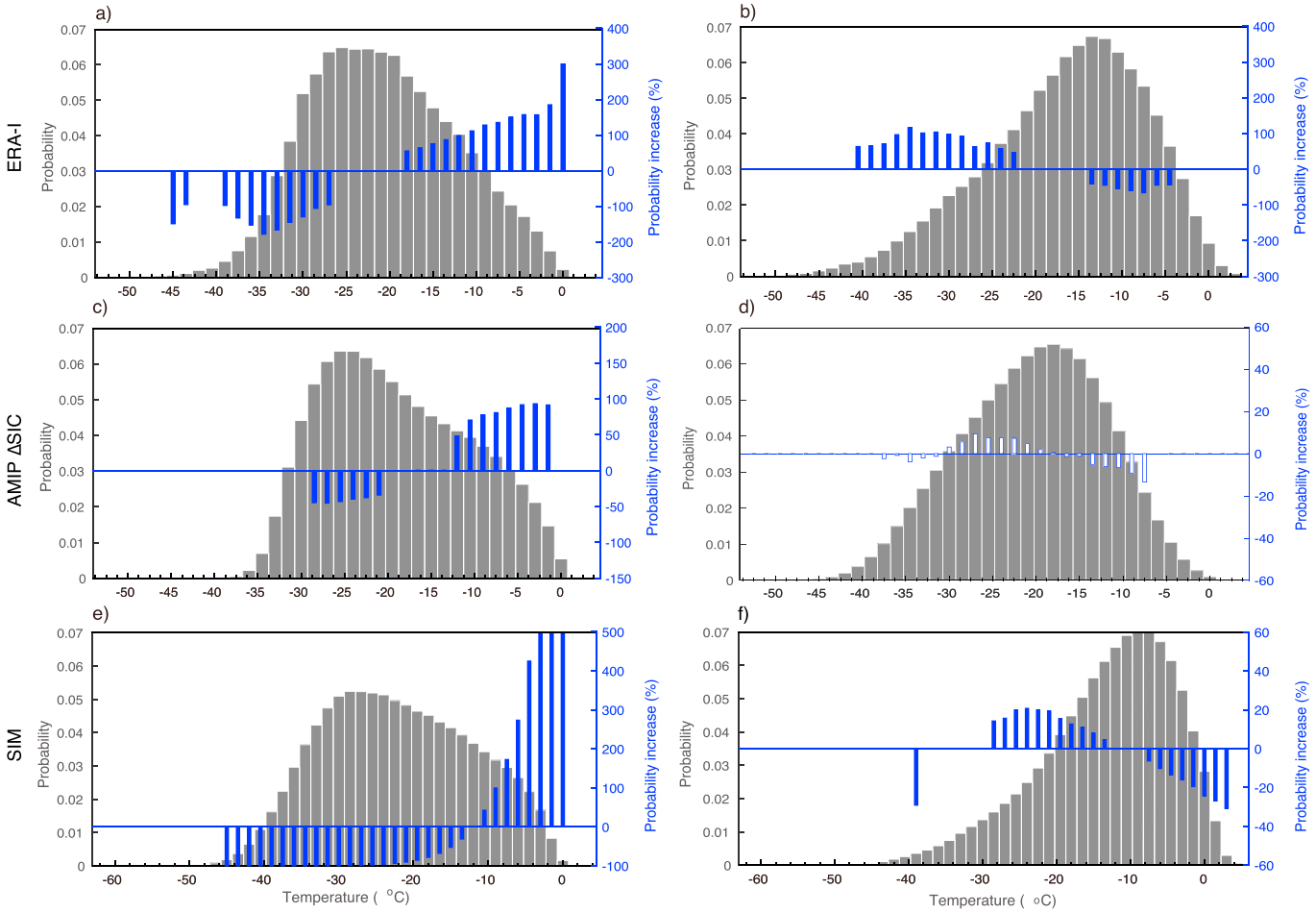

Figure 4. The probability distribution of daily surface temperature over the regions to the (a, c, and e) northwest (50°–70°E, 70°–80°N) and (b, d, f) southeast (75°–95°E, 48°–58°N) of I_{AN} center, respectively, for ERA-I (Figures 4a and 4b), AMIP ΔSIC (Figures 4c and 4d), and SIM (Figures 4e and 4f). The gray bars stand for the mean probability distribution and the blue bars for the changes of probability (%), computed as the linear trend or difference for each bin. The filled (open) bars indicate significant (insignificant) changes with respect to the top and lower 5th percentiles of the PDF from Monte Carlo resampling.

Acknowledgments

The authors thank the two anonymous reviewers for their very constructive comments, which help improve substantially the manuscript. This work is supported by the Office of Science of the U.S. Department of Energy (DOE) as part of the Regional and Global Climate Modeling (RGCM) program. D. Xue is supported by the China Scholarship Council. L. Sun is supported by the NOAA Climate Program Office. G. Chen is supported by DOE grant DE-SC0016117. Y. Zhang is jointly supported by the National Natural Science Foundation of China (grants 41475092 and 41621005) and the Jiangsu Collaborative Innovation Center for Climate Change. The ERA-I data are accessible from http://apps.ecmwf.int/datasets/data/interim-full-daily/levtype=sfc/. The data for ECHAM5 and CAM4 experiments can be found via site https://www.esrl.noaa.gov/psd/repository/alias/facts.

As far as the linkage between Arctic amplification and midlatitude weather extremes is concerned, this study should not be regarded conclusive. The total wave activity response to a polar thermal forcing is a nuanced one depending on how the midlatitude eddy-mean flow interaction responds to the thermal forcing and redistributes between the zonal mean momentum and wave activity. One should not confuse the redistribution under external forcing with the internal exchange in the absence of external forcing.

At issue is the model dependence of the atmospheric response to sea ice loss, and further model intercomparison study is in order. Meanwhile, the numerical experiments utilized in this study may not represent faithfully the true forcing from the sea ice melting [*Cohen et al.*, 2014; *Furtado et al.*, 2015]. Prescribing sea ice concentration and sea ice temperature may interfere the interactive nature of the air-ice heat exchange, and prescribing SST artificially excludes the ocean dynamical feedback (whose importance was acutely noted in *Deser et al.* [2015]). Further thoughtful, energetically consistent experimental designs with multiple models may lead to more definite attributions of the changes in the midlatitude extremes in the past and future.

References

Barnes, E. A. (2013), Revisiting the evidence linking Arctic amplification to extreme weather in midlatitudes, *Geophys. Res. Lett.*, *40*, 4734–4739, doi:10.1002/grl.50880.

Barnes, E. A., and J. A. Screen (2015), The impact of Arctic warming on the midlatitude jetstream: Can it? Has it? Will it?, *WIREs Clim. Change*, *6*, 277–286, doi:10.1002/wcc.337.

Chen, G., J. Lu, D. A. Burrows, and L. R. Leung (2015), Local finite-amplitude wave activity as an objective diagnostic of midlatitude extreme weather, *Geophys. Res. Lett.*, *42*, 10,952–10,960, doi:10.1002/2015GL066959.

Cohen, J., J. Jones, J. C. Furtado, and E. Tziperman (2013), Warm Arctic, cold continents: A common pattern related to Arctic sea ice melt, snow advance, and extreme winter weather, *Oceanography*, *26*(4), 150–160, doi:10.5670/oceanog.2013.70.
Cohen, J., et al. (2014), Recent Arctic amplification and extreme mid-latitude weather, *Nat. Geosci.*, *7*, 627–637, doi:10.1038/ngeo2234.
Coumou, D., and S. Rahmstorf (2012), A decade of weather extremes, *Nat. Clim. Change*, *2*, 491–496, doi:10.1038/nclimate1452.
Coumou, D., A. Robinson, and S. Rahmstorf (2013), Global increase in record-breaking monthly-mean temperatures, *Clim. Change*, *118*, 771–782, doi:10.1007/s10584-012-0668-1.
Dee, D. P., et al. (2011), The ERA-Interim reanalysis: Configuration and performance of the data assimilation system, *Q. J. R. Meteorol. Soc.*, *137*, 553–597, doi:10.1002/qj.828.
Delworth, T. L., F. Zeng, A. Rosati, G. A. Vecchi, and A. T. Wittenberg (2015), A link between the hiatus in global warming and north American drought, *J. Clim.*, *28*, 3834–3845, doi:10.1175/JCLI-D-14-00616.1.
Deser, C., R. A. Tomas, and L. Sun (2015), The role of ocean-atmosphere coupling in the zonal-mean atmospheric response to Arctic sea ice loss, *J. Clim.*, *28*, 2168–2186, doi:10.1175/JCLI-D-14-00325.1.
Francis, J. A., and S. J. Vavrus (2012), Evidence linking Arctic amplification to extreme weather in mid-latitudes, *Geophys. Res. Lett.*, *39*, L06801, doi:10.1029/2012GL051000.
Francis, J. A., and S. J. Vavrus (2015), Evidence for a wavier jet stream in response to rapid Arctic warming, *Environ. Res. Lett.*, *10*, doi:10.1088/1748-9326/10/1/014005.
Furtado, J. C., J. L. Cohen, A. H. Butler, E. E. Riddle, and A. Kumar (2015), Eurasian snow cover variability and Northern Hemisphere climate predictability, *Clim. Dyn.*, *45*, 2591–2605, doi:10.1029/1998GL900321.
Gerber, F., J. Sedláček, and R. Knutti (2014), Influence of the western North Atlantic and the Barents Sea on European winter climate, *Geophys. Res. Lett.*, *41*, 561–567, doi:10.1002/2013GL058778.
Graversen, R. G., T. Mauritsen, M. Tjernstrom, E. Kallen, and G. Svensson (2008), Vertical structure of recent Arctic warming, *Nature*, *451*, 53–56, doi:10.1038/nature06502.
Hassanzadeh, P., and Z. Kuang (2015), Blocking variability: Arctic amplification versus Arctic oscillation, *Geophys. Res. Lett.*, *42*, 8586–8595, doi:10.1002/2015GL065923.
Holland, M. M., and C. M. Bitz (2003), Polar amplification of climate change in coupled models, *Clim. Dyn.*, *21*, 221–232, doi:10.1007/s00382-003-0332-6.
Horton, D. E., N. C. Johnson, D. Singh, D. L. Swain, B. Rajaratnam, and N. S. Diffenbaugh (2015), Contribution of changes in atmospheric circulation patterns to extreme temperature trends, *Nature*, *522*, 465–469, doi:10.1038/nature14550.
Huang, C. S. Y., and N. Nakamura (2015), Local finite-amplitude wave activity as a diagnostic of anomalous weather events, *J. Atmos. Sci.*, doi:10.1175/JAS-D-15-0194.1.
Hurrell, J. W., J. J. Hack, D. Shea, J. M. Caron, and J. Rosinski (2008), A new sea surface temperature and sea ice boundary dataset for the Community Atmosphere Model, *J. Clim.*, *21*, 5145–5153, doi:10.1175/2008JCLI2292.1.
Inoue, J., M. E. Hori, and K. Takaya (2011), The role of Barents sea ice in the wintertime cyclone track and emergence of a Warm-Arctic Cold-Siberian anomaly, *J. Clim.*, *25*, 2561–2568.
Kretschmer, M., D. Coumou, J. F. Donges, and J. Runge (2016), Using causal effect networks to analyze different Arctic drivers of midlatitude winter circulation, *J. Clim.*, *29*, 4069–4081, doi:10.1175/JCLI-D-15-0654.1.
Kug, J.-S., J.-H. Jeong, Y.-S. Jang, B.-M. Kim, C. K. Folland, S.-K. Min, and S.-W. Son (2015), Two distinct influences of Arctic warming on cold winters over North America and East Asia, *Nat. Geosci.*, doi:10.1038/ngeo2517.
Li, C., B. Stevens, and J. Marotzke (2015), Eurasian winter cooling in the warming hiatus of 1998–2012, *Geophys. Res. Lett.*, *42*, 8131–8139, doi:10.1002/2015GL065327.
Liu, J., J. A. Curry, H. Wang, M. Song, and R. M. Horton (2012), Impact of declining Arctic sea ice on winter snowfall, *Proc. Natl. Acad. Sci. U.S.A.*, *109*, 4074–4079, doi:10.1073/pnas.1114910109.
McCusker, K. E., J. Fyfe, and M. Sigmond (2016), Twenty-five winters of unexpected Eurasian cooling unlikely due to Arctic sea-ice loss, *Nat. Geosci.*, *9*, 838–842, doi:10.1038/ngeo2820.
Min, S. K., X. Zhang, F. W. Zwiers, and G. C. Hegerl (2011), Human contribution to more-intense precipitation extremes, *Nature*, *470*, 378–381, doi:10.1038/nature09763.
Mori, M., M. Watanabe, H. Shiogama, J. Inoue, and M. Kimoto (2014), Robust Arctic sea-ice influence on the frequent Eurasian cold winters in past decades, *Nat. Geosci.*, *7*, 869–873, doi:10.1038/ngeo2277.
Nakamura, N., and A. Solomon (2010), Finite-amplitude wave activity and mean flow adjustments in the atmospheric general circulation Part 1. Quasigeostrophic theory and analysis, *J. Atmos. Sci.*, *67*, 3967–3983.
Nakamura, N., and D. Zhu (2010), Finite-amplitude wave activity and diffusive flux of potential vorticity in eddy-mean flow interaction, *J. Atmos. Sci.*, *67*(9), 2701–2716, doi:10.1175/2010JAS3432.1.
Overland, J. E., K. R. Wood, and M. Wang (2011), Warm Arctic-cold continents: Climate impacts of the newly open Arctic sea, *Polar Res.*, *30*, 15,787, doi:10.3402/polar.v30i0.15787.
Overland, J., J. Francis, R. Hall, E. Hanna, S. Kim, and T. Vihma (2015), The melting arctic and mid-latitude weather patterns: Are they connected?, *J. Clim.*, *28*, 7917–7932, doi:10.1175/JCLI-D-14-00822.1.
Perlwitz, J., M. Hoerling, and R. M. Dole (2015), Arctic tropospheric warming: Causes and linkages to lower latitudes, *J. Clim.*, *28*, 2154–2167, doi:10.1175/JCLI-D-14-00095.1.
Petoukhov, V., and V. A. Semenov (2010), A link between reduced Barents-Kara sea ice and cold winter extremes over northern continents, *J. Geophys. Res.*, *115*, D21111, doi:10.1029/2009JD013568.
Screen, J. A., and I. Simmonds (2010), Increasing fall-winter energy loss from the Arctic Ocean and its role in Arctic temperature amplification, *Geophys. Res. Lett.*, *37*, L16797, doi:10.1029/2010GL044136.
Screen, J. A., and I. Simmonds (2013), Exploring links between Arctic amplification and mid-latitude weather, *Geophys. Res. Lett.*, *40*, 959–964, doi:10.1002/grl.50174.
Screen, J. A., and I. Simmonds (2014), Amplified mid-latitude planetary waves favour particular regional weather extremes, *Nat. Clim. Change*, *4*, 704–709, doi:10.1038/nclimate2271.
Screen, J. A., C. Deser, I. Simmonds, and R. Tomas (2013), Atmospheric impacts of Arctic sea-ice loss, 1979–2009: Separating forced change from atmospheric internal variability, *Clim. Dyn.*, *43*, 333–344, doi:10.1007/s00382-013-1830-9.
Serreze, M., A. Barrett, and J. Stroeve (2009), The emergence of surface-based Arctic amplification, *Cryosphere*, *3*, 11–19, doi:10.5194/tc-3-11-2009.
Sillmann, J., M. Corci-Maspoli, M. Kallache, and R. W. Katz (2011), Extreme cold winter temperatures in Europe under the influence of North Atlantic atmospheric blocking, *J. Clim.*, *24*, 5899–5913, doi:10.1175/2011JCLI4075.1.

Sun, L., J. Perlwitz, and M. Hoerling (2016), What caused the recent "warm Arctic, cold continents" trend pattern in winter temperatures?, *Geophys. Res. Lett.*, *43*, 5345–5352, doi:10.1002/2016GL069024.

Tang, Q., X. Zhang, X. Yang, and J. A. Francis (2013), Cold winter extremes in northern continents linked to Arctic sea ice loss, *Environ. Res. Lett.*, *8*, doi:10.1088/1748-9326/8/1/014036.

Westra, S., L. V. Alexander, and F. W. Zwiers (2013), Global increasing trends in annual maximum daily precipitation, *J. Clim.*, *26*, 3904–3918, doi:10.1175/JCLI-D-12-00502.1.